

A SHOCK-INDUCED PDR IN THE HH 80/81 FLOW. FAR INFRARED SPECTROSCOPY.⁰

SERGIO MOLINARI

Infrared Processing and Analysis Center, California Institute of Technology, MS 100-22, Pasadena, CA 91125, USA

Electronic mail: molinari@ipac.caltech.edu

ALBERTO NORIEGA-CRESPO

SIRTF Science Center, California Institute of Technology

IPAC 100-22, Pasadena, California, 91125

Electronic mail: alberto@ipac.caltech.edu

&

LUIGI SPINOGLIO

CNR-Istituto di Fisica dello Spazio Interplanetario, Area di Ricerca Tor Vergata, via Fosso del Cavaliere I-00133 Roma, Italy

Electronic mail: luigi@ifsi.rm.cnr.it

Accepted 2000 August 24

ABSTRACT

The two spectrometers on board the Infrared Space Observatory were used to observe the Herbig-Haro objects HH 80, 81 and 80N, as well as their candidate exciting source IRAS 18162-2048. The fine structure lines of [OI]63 μ m, [OI]145 μ m and [CII]158 μ m are detected everywhere, while [NII]122 μ m and [OIII]88.3 μ m are only detected toward the HH objects; line ratios confirm for the first time the collisionally excited HH nature of HH 80N. No molecular line is detected in any of the observed positions. We use a full shock code to diagnose shock velocities $v_s \sim 100$ km s⁻¹ toward the HH objects, as expected from the optical spectroscopy. Since proper motions suggest velocities in excess of 600 km s⁻¹, the HH objects probably represent the interface between two flow components with velocity differing by $\sim v_s$. Aside from the flow exciting source, the [CII]158 μ m line is everywhere brighter than the [OI]63 μ m line, indicating the presence of a Photo-Dissociation Region (PDR) all along the flow. Continuum emission from the HH objects and from other positions along the flow is only detected longward of $\sim 50\mu$ m, and its proportionality to the [CII]158 μ m line flux suggests it is PDR in origin. We propose that the FUV continuum irradiated by the HH objects and the jet is responsible for the generation of a PDR at the walls of the flow cavity. We develop a very simple model which strengthens the plausibility of this hypothesis.

Subject headings: Stars: formation - (ISM:) Herbig-Haro objects - ISM: individual objects: HH 80/81 - Infrared: ISM: lines and bands

1. INTRODUCTION

Stellar jets and outflows arising from low mass protostellar objects are considered ubiquitous, since essentially each protostar must go through an active period of mass loss to get rid of its angular momentum to become a star (c.f. Hartmann 1998). These outflows are well collimated and supersonic and interact mostly through shocks with the interstellar medium. When these shock ex-

cited regions are detected by optical means, they are identified as Herbig-Haro objects (Reipurth & Heathcote 1997).

The process of mass loss for intermediate and high mass protostellar objects is less well understood (Churchwell 1998). Observationally very few of these objects have collimated optical jets or well defined molecular outflows (Poetzel, Mundt & Ray 1989; Shepherd & Churchwell 1996). The

⁰Based on observations with ISO, an ESA project with instruments funded by ESA Member States (especially the PI countries: France, Germany, the Netherlands and the United Kingdom) with the participation of ISAS and NASA.

Herbig-Haro 80-81 system, which is driven by a $20\,000\,L_{\odot}$ IRAS source, is one of those rare cases with a well collimated supersonic jet that reaches flow velocities of $\sim 600 - 1400\,\text{km s}^{-1}$ (Martí et al. 1995, 1998). HH 80/81 are at the edge of the L291 cloud in Sagittarius (Reipurth & Graham 1988) at an estimated kinematical distance of 1.7 kpc (Rodríguez et al. 1980). At this distance the HH 80/81 system, with an angular size of $\sim 10''.8$, spans ~ 5.3 pc. The proper motion measurements confirm that IRAS 18162-2048 is the source driving the outflow, which is part of a small cluster of infrared sources (Aspin & Geballe 1992; Aspin et al. 1994). IRAS 18162-2048, given its large luminosity, is likely to become a B type star. Most of the early work on HH 80/81 was performed at radio wavelengths, where 3.6 and 6 cm observations found the collimated radio jet emanating from IRAS 18162-2048, as well as a section of the counter-flow, named HH 80N, which is optically invisible (Rodríguez & Reipurth 1989; Martí, Rodríguez & Reipurth 1993, hereafter MRR93).

Recently Heathcote, Reipurth & Raga (1998, hereafter HRR) have carried a detailed analysis of HH 80/81 morphology and kinematics, using HST WFPC2 images and ground based optical images and spectra. They concluded in their study that the emission arising from HH 80/81 is due to shocks with velocities up $600\,\text{km s}^{-1}$. The energy release by such shocks is so high that thermalizes the gas to temperatures $> 10^6\,\text{K}$, i. e. the shocks are adiabatic. If the HH objects were to resemble bow shock structures (Raga & Böhm 1986; Hartigan et al. 1987), then the optical emission observed in $\text{H}\alpha$ or $[\text{OIII}]\,\lambda 5007$ comes from the ‘wings’, while the stagnation region (the tip of the bow) is several times further ahead and invisible. This scenario, however, is derived by modeling the optical line profiles (HHR98); from the morphological viewpoint, the HH objects appear as irregular knots that do not resemble wings of a bow.

In this study we present ISO (Kessler et al. 1996) spectroscopic observations of the HH 80/81/80N system, including their exciting source IRAS 18162-2048. The observations and data analysis are presented in §2 and the results in §3. A model to interpret the results is pre-

sented in §4 and discussed in §5. We summarize our conclusions in §6.

2. OBSERVATIONS

We used the two spectrometers on the ISO satellite to observe several locations along the HH 80/81 flow, including the candidate exciting source IRAS 18162-2048. The Long Wavelength Spectrometer (LWS, Clegg et al. 1996) was used in its LWS01 grating mode to acquire full low resolution ($R \sim 200$) $43\text{--}197\,\mu\text{m}$ scans. Data were collected every $1/4$ of a resolution element (equivalent to $\sim 0.07\,\mu\text{m}$ for $\lambda \lesssim 90\,\mu\text{m}$, and to $\sim 0.15\,\mu\text{m}$ for $\lambda \gtrsim 90\,\mu\text{m}$) with 0.5s integration time; a total of 24 scans were accumulated, corresponding to 48s integration time per spectral element. LWS data processed through Off-Line Processing (OLP), version 7, have been reduced using the LWS Interactive Analysis¹ (LIA) Version 7.2. The dark current and gain for each detector were re-estimated, and the data were recalibrated in wavelength, bandpass and flux. The absolute flux calibration for LWS in grating mode is 10% (ISO Handbook, iv, 4.3.2).

The Short Wavelength Spectrometer (SWS, de Graauw et al. 1996) was used in its SWS01 ‘Speed 2’ grating mode. In this mode the grating is moved faster than the detector reset time, with a loss of about a factor 7 (ISO Handbook, vi 3.3) in achievable spectral resolution, resulting in $R \sim 300$. The total observing time was about 1900s. SWS data were processed using OSIA, the SWS Interactive Analysis². Dark currents and photometric checks were revised. The March 1998 bandpass calibration files have been used to produce the final spectra. The accuracy of the SWS absolute flux calibration varies between 7% and 35% from 2 to $40\,\mu\text{m}$ (ISO Handbook, vi 5.4.2).

The final steps of data analysis were done using the ISO Spectral Analysis Package³ (ISAP) Version 1.6a for both LWS and SWS. Grating scans (LWS) and detectors spectra (SWS) were averaged using a median clipping algorithm optimised to flag and discard outliers mainly due to transients. The LWS spectra were heavily fringed, and standard techniques available under ISAP were used to remove these instrumental effects. Line fluxes were estimated by means of gaussian fit-

¹LIA is available at <http://www.ipac.caltech.edu/iso/lws/lia/lia.html>

²OSIA is available at http://www.mpe.mpg.de/www_ir/ISO/observer/osia/osia.html

³ISAP is available at <http://www.ipac.caltech.edu/iso/isap/isap.html>

TABLE 1

Observations

Object		α (B1950)	δ (B1950)	AOTs & TDTs
IRAS 18162-2048	ON	18 16 12.9	−20 48 49	LWS01-32901362
	OFF S	18 16 12.9	−20 50 29	LWS01-32901362
	OFF N	18 16 12.9	−20 47 09	LWS01-32901362
HH 80		18 16 06.8	−20 53 06	LWS01-32901350, SWS01-32901351
HH 81		18 16 07.4	−20 52 23	LWS01-32901360, SWS01-32901361
HH 80N		18 16 20.7	−20 42 53	LWS01-32901363

ting.

Table 1 lists the observed positions, which are also reported in Fig. 1 as the centers of the dashed circles (the LWS FWHM beamsize) superimposed on the 6 cm VLA map of MRR93). The last column reports the Astronomical Observation Template (AOT) used, together with the 8-digits unique identifier of the observation (TDT).

3. RESULTS

All objects were detected with the LWS, while no line or continuum is detected with the SWS toward HH 80 and 81. Table 2 lists the measured fluxes for the detected lines; upper limits are given at the 1σ level. The distance between HH 80 and 81 is about one half of the LWS beamsize ($\sim 80''$ FWHM at most wavelengths, see ISO Handbook, IV 4.10.1) implying that each object contributes roughly half of its flux (lines and continuum) to the observed flux of its neighbour. Contamination corrected fluxes for HH 80 and 81 are listed just below the observed ones for each line.

A glance at Table 2 is sufficient to identify the basic results of our observations and set the guidelines for the interpretation of our data. First of all we note that the [NII]122 μ m and [OIII]88.3 μ m lines are only detected toward the HH objects; these observations provide the first direct evidence for the collisionally excited HH nature of HH 80N. Although the LWS pointing toward IRAS 18162-2048 encompasses the radio-brightest portions of the thermal jet, no lines from ionised species (other than [CII]158 μ m, but see below) are detected. We verified that the [NII]122 μ m and [OIII]88.3 μ m lines detected toward the HH objects would still be detectable toward IRAS 18162-2048, in spite of the higher photon noise from this

more intense continuum source. Secondly, molecular emission is not detected anywhere. Finally we note that with the exception of IRAS 18162-2048, the [CII]158 μ m line is everywhere brighter than the [OI]63 μ m line. The detected lines are reported in Fig. 2 for the HH objects pointings, and in Fig. 3 for the three central observed positions of the flow.

3.1. The Herbig-Haro Objects

The HH 80/81 system is the most powerful flow known to emanate from an intermediate mass Young Stellar Object (YSO). Velocities in excess of 600 km s $^{-1}$ are derived from proper motion measurements both in radio continuum (Martí, Rodríguez & Reipurth 1995, 1998) and optical lines (HRR). In addition, line profile analysis of high-dispersion optical spectra suggests shock velocities $v_s \sim 650$ km s $^{-1}$ (HRR). Interestingly enough however, optical spectra only reveal lines from species up to double ionisation state. Our FIR spectroscopy has the immediate advantage that reddening corrections, which are critical in the optical regime especially in this highly extinguished region (HRR), are not important. To diagnose the shock conditions toward HH 80, 81 and 80N, we compare our observations with the predictions from plane parallel atomic shock models. The shock models were calculated using MAP-PINGS2, a code developed by Binette et al. (Binette, Dopita, & Tuohy 1985), which has been thoroughly tested (Pequignot 1986).

A grid of models was created changing the pre-shock density between 10^2 and 10^4 cm $^{-3}$, consistent with values derived by HRR from optical lines analysis. Shock velocity were varied between 60 and 110 km s $^{-1}$; higher values, although

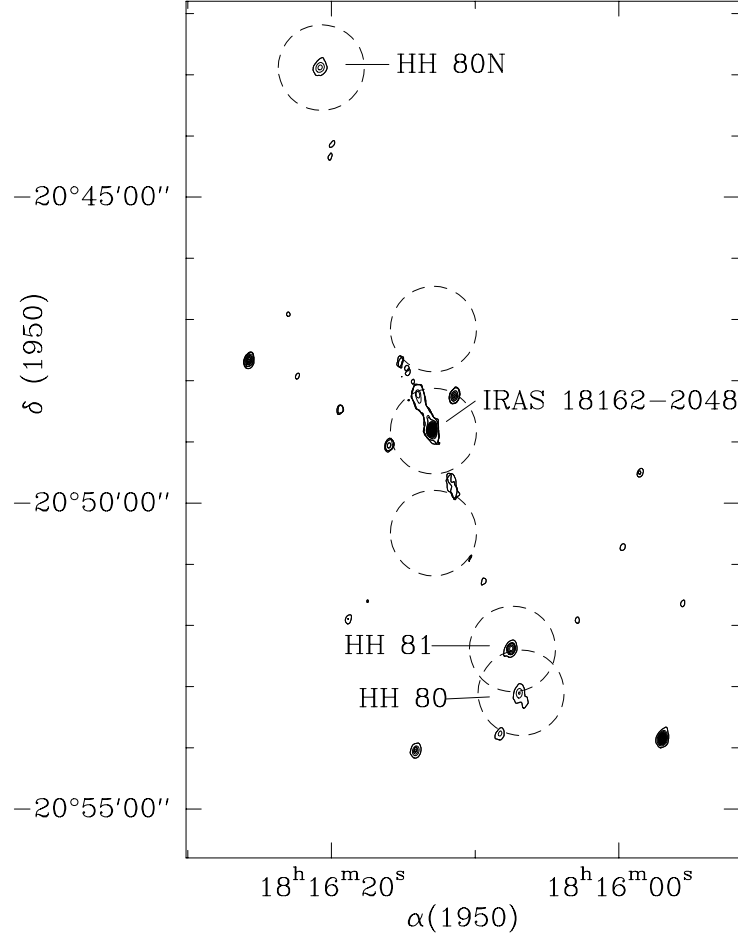


FIG. 1.— VLA 6 cm composite map of the HH 80/81 region (Martí, Rodríguez & Reipurth (1993), courtesy of L.F. Rodríguez); superimposed is the ISO-LWS field of view (dashed circles) at all observed positions. The various sources in the field are labeled.

TABLE 2

Observed Line Fluxes^a

Line	ON	IRAS 18162-2048		HH 80	HH 81	HH 80N
		OFF S	OFF N			
[OI]63 μ m	104(2)	7.1(0.5)	8.0(0.3)	6.4(0.2) 3.8 ^b	7.1(1.0) 5.2 ^b	8.2(0.2)
[OI]145 μ m	10.6(0.7)	0.3(0.1)	1.0(0.2)	0.4(0.1) 0.3 ^b	0.32(0.04) 0.16 ^b	0.7(0.2)
[OIII]88.3 μ m	≤ 4	≤ 0.3	≤ 0.4	0.8(0.4) 0.4 ^b	1.0(0.4) 0.8 ^b	1.0(0.2)
[NII]122 μ m	≤ 1	≤ 0.3	≤ 0.2	0.35(0.08) 0.11 ^b	0.53(0.07) 0.47 ^b	0.7(0.1)
[CII]158 μ m	37(1)	16.3(0.3)	20.4(0.3)	11.49(0.06) 6.97 ^b	12.53(0.08) 9.04 ^b	17.1(0.1)

^a Units of 10^{-19} W cm $^{-2}$ and 1σ statistical uncertainties in parenthesis; upper limits are at the 1σ level.

^b Contamination-corrected fluxes.

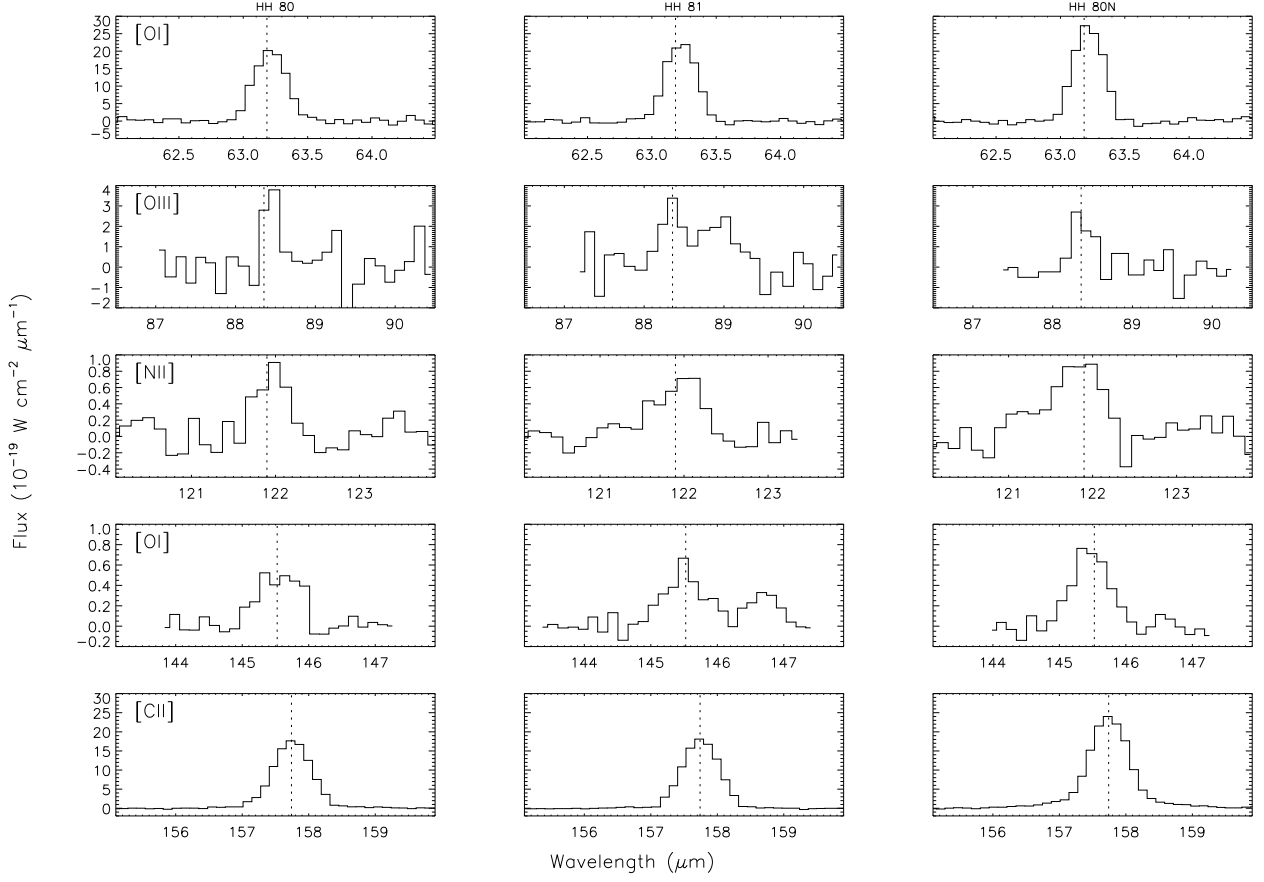


FIG. 2.— Detected lines toward HH 80, 81 and 80N. Flux densities are normalised to $10^{-19} \text{ W cm}^{-2} \mu\text{m}^{-1}$. The dotted vertical lines represent the expected linecenter wavelength.

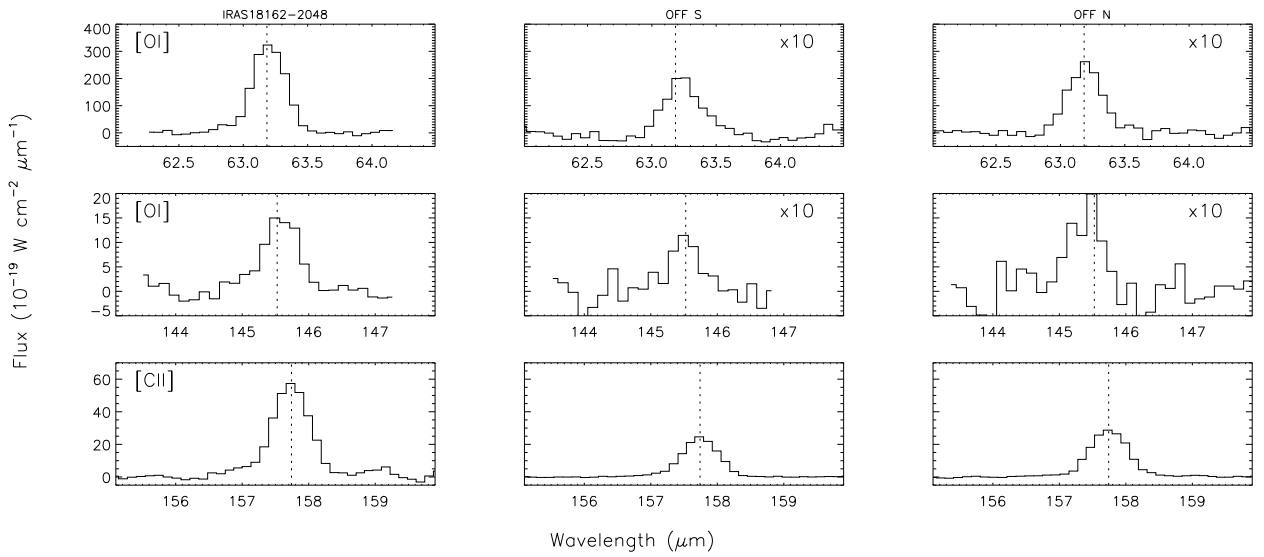


FIG. 3.— Detected lines toward IRAS 18162-2048, OFF S and OFF N. Flux densities are normalised to $10^{-19} \text{ W cm}^{-2} \mu\text{m}^{-1}$. The dotted vertical lines represent the expected linecenter wavelength.

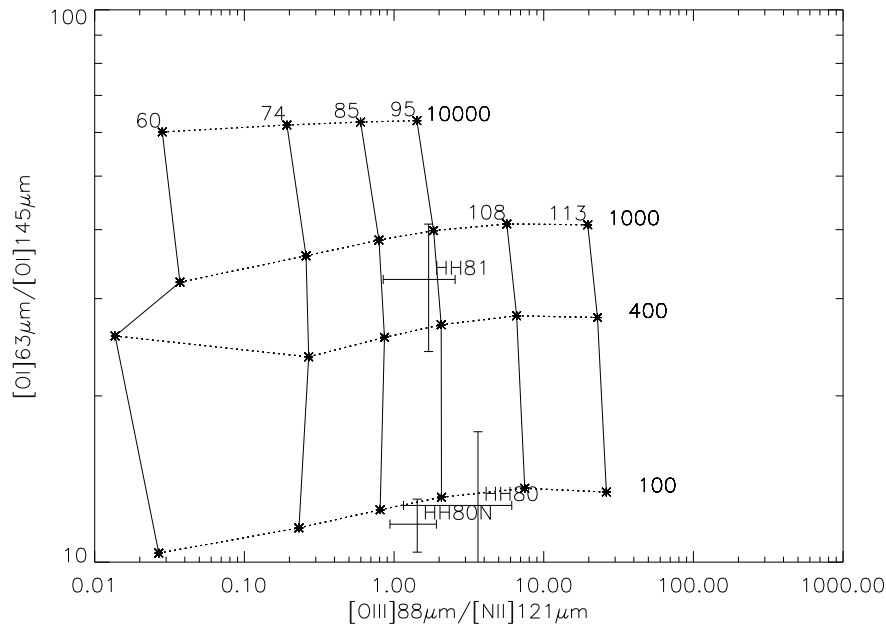


FIG. 4.— $[\text{OI}]63\mu\text{m}/[\text{OI}]145\mu\text{m}$ vs $[\text{OIII}]88.3\mu\text{m}/[\text{NII}]121\mu\text{m}$ diagnostic diagram obtained from the models of Binette et al. 1985. Horizontal lines are of constant pre-shock density (in cm^{-3}), while vertical lines are of constant shock velocity (in km s^{-1}).

still compatible with results from optical line ratios (HRR), fail to produce lines like $[\text{NII}]122\mu\text{m}$ and $[\text{OIII}]88.3\mu\text{m}$ which are instead observed toward the HH objects. The preshock degree of ionisation and magnetic field strength were kept fixed at 0.1 and $10\mu\text{G}$ respectively. These values are not critical for the velocities we used (but see HRR § 8.2) and represent typical values for stellar jets (but see Bacciotti & Eisloffel 1999) from low-mass YSOs; we will assume they are also valid for higher-mass systems like the one we are presently dealing with. This selection of initial values also allow us to gauge our models with those of Hartigan, Raymond and Hartmann (1987). In all instances solar abundances were used, since this is a reasonable assumption for Herbig-Haro objects (Beck-Winchatz, Böhm, Noriega-Crespo 1996). Fig. 4 clearly show that shock velocities between 90 and 110 km s^{-1} are appropriate to reproduce the emitted spectra for all HH objects. Pre-shock densities between 100 and 1000 cm^{-3} are derived, in full agreement with estimates from HRR. In these conditions of low density J-shocks (Draine 1980) negligible cooling is expected from molecular lines like CO, H_2 and H_2O (Hollenbach & McKee 1989), in agreement with our observations. Furthermore, the absence of FIR molecular emission also rules out

the presence of a significant C-type shock component, for which H_2 , CO and H_2O molecular lines would be the main coolants (e.g., Kaufman & Neufeld 1996).

These low velocity shocks plus the width of the observed optical lines suggested to HHR that the HH 80/81 objects correspond to “wings” of a highly adiabatic bow shock that strikes the surrounding gas at $\sim 650 \text{ km s}^{-1}$; in such wings the shock front would be oblique with respect to the direction of motion, resulting in lower shock velocities. A shock velocity of $\sim 100 \text{ km s}^{-1}$ and flow velocities (from the proper motions) as high as 600 km s^{-1} can be also reconciled if one considers that the mass loss from the protostar is time dependent, and that the observed configuration of HH 80/81 was preceded by previous ejection events. If this is the case, the new ejected gas finds the circumstellar gas already in motion, and it is the interaction between these two flows that can create relative shock velocities of $\sim 100 \text{ km s}^{-1}$ or so (Raga et al. 1990; Stone & Norman, 1993). Multi-epoch VLA observations (Martí, Rodríguez & Reipurth 1995, 1998) of the jet’s radio knots provide supporting evidence for episodic mass loss from IRAS 18162-2048.

A similar process has been invoked to understand the flow characteristics of the HH 1/2 sys-

tem, where the proper motions are as high as 450 km s^{-1} in both atomic and molecular H_2 gas (Herbig & Jones 1981; Rodríguez et al. 1990; Eislöffel, Mundt & Böhm 1994; Noriega-Crespo et al. 1997), but the shock themselves are $\sim 150 - 200 \text{ km s}^{-1}$ (Hartigan et al. 1987; Noriega-Crespo, Böhm & Raga 1989). In the HH 1/2 outflow, however, there is clear evidence of a previous outburst event marked by the presence of an older bow shock structure ~ 10 times farther away from central outflow source (Ogura 1995).

3.2. *The Jet*

The LWS pointing toward IRAS 18162-2048 encompasses the base of the radio thermal jet, which is the strongest radio emitter in the flow. Yet no $[\text{OIII}]88.3\mu\text{m}$ or $[\text{NII}]122\mu\text{m}$ emission is detected, indicating that the ionised material of the jet is at a lower temperature compared to HH 80, 81 and 80N, or that the ionisation does not result from shocks. Interestingly, the radio spectral index of the jet is consistent with that of an ionised wind, but significantly differs from that of the HH objects which instead manifest a possible synchrotron component (MRR93). This behavior is different from that of the HH 1/2 system, for instance, where the central source VLA 1 (Pravdo et al. 1985) has a similar positive radio spectral index to that of HH 80/81 jet, but for the HH objects themselves it is flat, indicating optically thin free-free emission (Rodríguez et al. 1990).

3.3. *The PDR*

In the shock conditions diagnosed by our FIR spectroscopy (see Sect. 3.1), $[\text{CII}]158\mu\text{m}$ contributes about 20% of the $[\text{OI}]63\mu\text{m}$ cooling. Since $[\text{CII}]158\mu\text{m}$ is everywhere brighter than $[\text{OI}]63\mu\text{m}$ (except toward IRAS 18162-2048) the $[\text{CII}]158\mu\text{m}$ emission must have another origin, namely PDR. Evidence for a PDR-like emission is also offered by the FIR continua detected toward the HH object and the OFF positions (the latter cannot be entirely justified with contamination by the stronger continuum source IRAS 18162-2048). Fig. 5 shows the SEDs observed toward all pointed positions with the LWS. We note that the continuum observed toward the two OFF positions cannot be justified with contamination from IRAS 18162-2048. The continua from HH 80 and 81 have been corrected for reciprocal contamination (see end of §2), and detector spectra have been stitched for cosmetic purposes.

In a PDR, electrons are released in the gas phase by FUV-irradiated dust grains via the photoelectric effect and heat the gas (Tielens & Hollenbach 1985). Theory and observations generally agree on the fact that between 0.1% and 1% of the incident FUV flux is converted into gas heating via this mechanism, and subsequently released mainly via “cooling” of the $[\text{CII}]158\mu\text{m}$ line. The rest of the incident field is absorbed by dust and reprocessed to FIR wavelengths. We see from Fig. 5 that the observed SEDs contain the bulk of FIR emission, so that their integral is a good representation of the reprocessed FUV field; the ratio of observed $[\text{CII}]158\mu\text{m}$ to the integrated SEDs yields values $0.002 \leq \chi_c \leq 0.013$, in very good agreement with expectations for a PDR. The only obvious exception is IRAS 18162-2048, whose SED is dominated by radiation from the central YSO.

Assuming that the pre-shock densities diagnosed for the HH objects (Sect. 3.1) represent the average conditions surrounding the HH 80/81 flow, we can use the observed $[\text{CII}]158\mu\text{m}$ flux to estimate the intensity of the irradiating FUV field. Using the Web Infrared Tool Shed (Wolfire et al.) and assuming complete filling of the LWS beam with filling factor of unity we estimate $G_0 \sim 200, 400, 30\,000, 200, 40$ and 30 for the 6 LWS pointings from north to south (see Fig. 1), where G_0 is the FUV field intensity expressed in units of $1.6 \times 10^{-3} \text{ ergs cm}^{-2} \text{ s}^{-1}$ (Habing 1968). In these conditions the PDR emission could account for most of the $[\text{OI}]63\mu\text{m}$ and $[\text{OI}]145\mu\text{m}$ fluxes everywhere along the flow, including the HH objects. In this case the $[\text{OI}]63\mu\text{m}/[\text{OI}]145\mu\text{m}$ ratios would imply densities $n < 10^4 \text{ cm}^{-3}$.

We searched several degrees around the HH 80/81 area for OB stars which could be responsible for this irradiation level, finding none. An obvious candidate is of course IRAS 18162-2048 itself. Assuming a B0 ZAMS spectral class (MRR93), the resulting FUV field at the various LWS pointings would be $G_0 \sim 450$ at OFF-N and OFF-S, and ~ 60 at the HH objects; the agreement with the G_0 values estimated from the $[\text{CII}]158\mu\text{m}$ line can be considered satisfactory. K-band images of IRAS 18162-2048, however, clearly resolve the IRAS source in a small cluster of at least 3 sources (Aspin et al. 1994); redistribution of the total bolometric luminosity of the IRAS source among the cluster members, adopting the

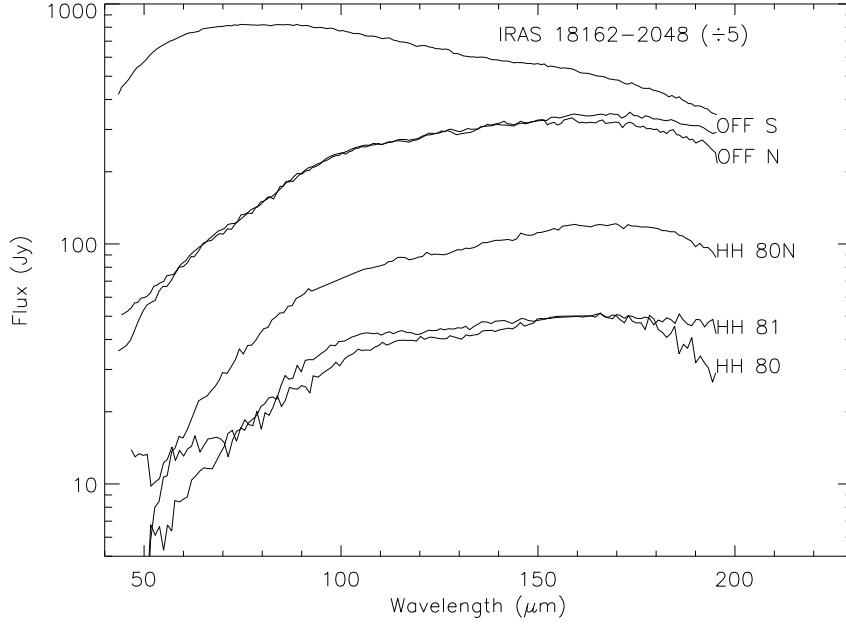


FIG. 5.— Spectral energy distributions observed with LWS toward all pointings. The SED from IRAS 18162-2048 has been divided by 5 to fit it into the plot range. The SEDs of HH 80 and 81 have been corrected for reciprocal contamination.

IMF from Miller & Scalo (1979), would assign only half of this luminosity to the most massive member of the cloud (e.g., Molinari et al. 2000, and references therein). This decreases the Lyman continuum photon flux by more than one or-

der of magnitude and reduces G_0 by nearly two orders of magnitude, ruling out IRAS 18162-2048 as the PDR illuminating source.

An intriguing possibility is that the illuminating sources for the observed PDR emission are

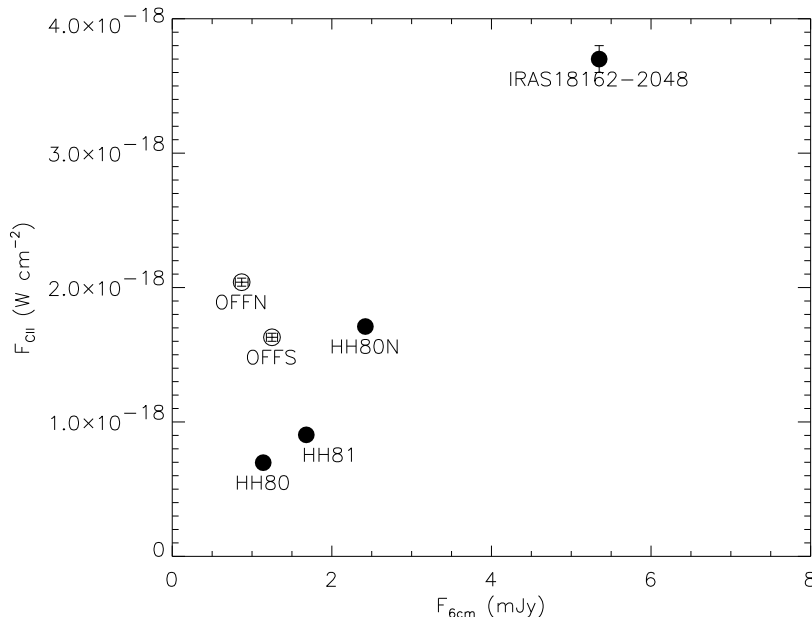


FIG. 6.— Plot of the [CII]158 μ m line flux *vs* the 6 cm continuum flux from the knots of the jet encompassed by the LWS beam. When errorbars are not visible is because they are smaller than the symbols.

the HH objects and the jet. In Fig. 6 we report the $[\text{CII}]158\mu\text{m}$ line flux as a function of the 6 cm flux measured by MRR93. The filled symbols represent the HH objects and IRAS 18162-2048; for each object we consider the radio knots encompassed by the LWS beam at each position. The correlation between F_{CII} and $F_{6\text{cm}}$ would seem to suggest that the ionised material and the amount of cooling by the PDR maybe somehow related. We note that the two OFF positions do not fit with the correlation in Fig. 6. In the next paragraph we will propose a semi-empirical model to verify and quantify the Radio-PDR connection.

4. A MODEL FOR THE SHOCK/JET-PDR CONNECTION

The influence of shock-originated radiation on the surrounding medium in HH flows is not clear. NH_3 and HCO^+ enhancements have been detected in the vicinity of HH 80N, HH 1 and HH 2 (Girart et al. 1994, 1998; Davis, Dent & Bell Burnell 1990; Torrelles et al. 1992, 1993) and it has been suggested that the UV field generated in the HH shocks may be responsible. Wolfire & Königl (1993), and more recently Raga & Williams (2000), have shown that the chemistry of blobs in the vicinity of HH objects can be influenced by the passage of the HH object, although the predicted morphologies do not match the observations.

We propose a scenario where the ionised material which is recombining behind the shock front and in the jet, and which emits free-free radio continuum, is also responsible for a UV field which illuminates internally the walls of the flow cavity; a PDR is there produced, which mainly cools via the $[\text{CII}]158\mu\text{m}$ line. If this is correct, then we should be able to express the two observables, i.e. the radio continuum flux and the $[\text{CII}]158\mu\text{m}$ line flux, as a function of a set of physical parameters which characterize the HH shocks, the jet and the PDR.

Radio emission from shocked material has been modeled by Curiel, Cantó and Rodríguez (1987); in the optically thin regime, the free-free emission from the recombination region can be written as

$$S_{sh\nu} = 1.84 \cdot 10^{-4} \theta^2 \left[\frac{\nu}{10 \text{ GHz}} \right]^{-0.1} T_4^{0.45} n_{o10} v_{s7} [1 + 3.483 v_{s7} - 2.745] \text{ mJy} \quad (1)$$

where θ is the angular diameter in seconds of arc of the recombination region, T_4 is the electrons temperature in units of 10^4K , n_{o10} is the pre-shock density in units of 10 cm^{-3} , and v_{s7} is the shock velocity in units of 100 km s^{-1} . This model applies to HH 80, 80N and 81, whose high ionization lines clearly trace a high velocity shock. In the absence of similar evidence toward the central source and the two OFF positions (Tab. 2), where the LWS beam encompasses most of the jet radio knots, we will assume that the ionisation does not results from shocks. Reynolds (1986) developed a model to predict the properties of radio continuum emission from a collimated, ionised thermal jet. His expression of the radio flux at any specific frequency is a complicated function of jet parameters like the collimation, the density, temperature and ionization radial gradients, the initial distance where the jet is injected, the jet's width at its base. Because we cannot independently fix any of these parameters, the diagnostic power of this model will be very limited in the present case.

Let us now quantify the energy released by the shock recombination region, in the portion of the UV continuum, between 912\AA and 2066\AA (or between 13.6eV and 6eV), which is effective in PDR illumination. It is widely accepted (Dopita, Binette & Schwartz 1982) that the dominant contribution to UV continuum in this wavelength range comes from hydrogenic $2s \rightarrow 1s$ two-photon decay. Theoretical models (Shull & McKee 1979, also confirmed by our grid of computed shock models (§3.1)) suggest that two-photon emission from He^0 and He^+ can be neglected in comparison. The H^0 two-photon emissivity is given by

$$j_\nu = \frac{1}{4\pi} \frac{h\nu}{\nu_0} P_{\nu/\nu_0} N_{2s} \text{ erg s}^{-1} \text{ sr}^{-1} \text{ cm}^{-3} \text{ Hz}^{-1} \quad (2)$$

where ν_0 is the $\text{Ly}\alpha$ frequency. P_{ν/ν_0} is the probability, symmetrical around $\frac{1}{2}\nu_0$, that a photon is emitted with frequency ν/ν_0 and for which we adopted the analytical approximation of Nussbaumer & Schmutz (1984). N_{2s} is the population density of level 2s and can be found equating the recombination rate from higher states to 2s, with the total $2s \rightarrow 1s$ two-photon decay rate. We obtain (Emerson 1996):

$$N_{2s} \sim 0.3 \alpha'_{rec} N_e N_i A_{2q}^{-1} \text{ cm}^{-3} \quad (3)$$

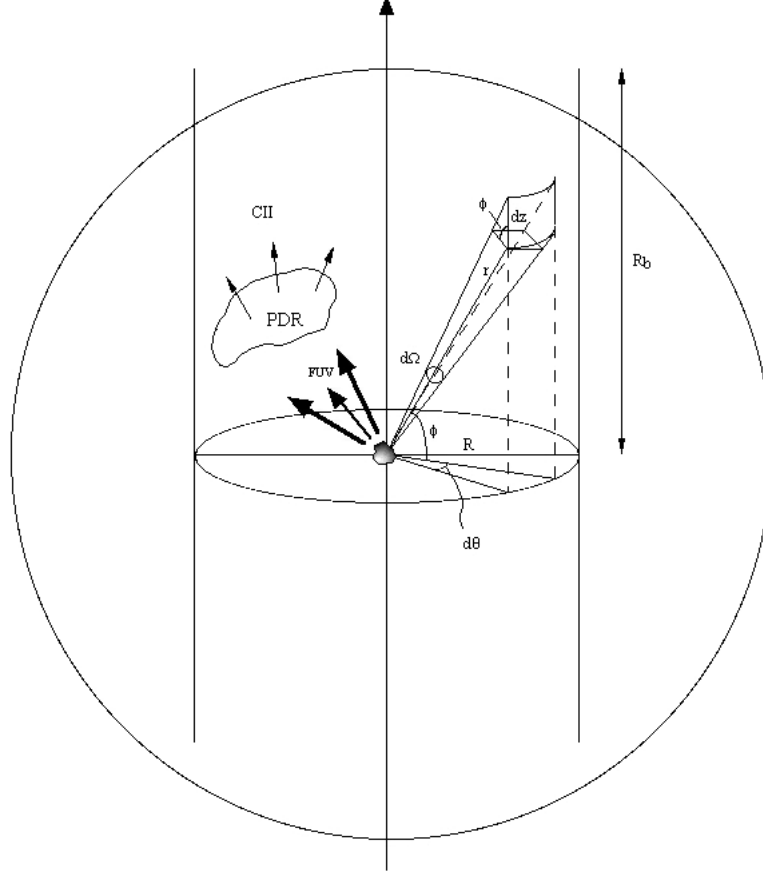


FIG. 7.— Sketch of the proposed scenario for the HH-PDR connection. The HH object is the grey knot at the origin of the coordinate system, and the cylinder represents the cavity excavated by the flow. The portion of big circle at the top of the figure indicates the ISO-LWS beam.

where N_e and N_i are the electron and ion number densities, and $A_{2q} \sim 8.23 \text{ s}^{-1}$ is the two-photon transition probability. The total recombination coefficient to all hydrogen excited levels can be written as (Hummer & Seaton 1963):

$$\alpha'_{rec} = 1.627 \cdot 10^{-13} T_4^{-1/2} [1 - 1.657 \text{Log}_{10} T_4 + 0.584 T_4^{1/3}] \text{ cm}^3 \text{ s}^{-1} \quad (4)$$

where T_4 is $T/10^4 \text{ K}$. Using Eqs. (2), (3) and (4), we are able to write the power radiated by the recombination region in the FUV as:

$$L_{FUV} = 4\pi V_{rec} \eta_{ce} \int_{6\text{eV}}^{13.6\text{eV}} j_\nu d\nu \text{ erg s}^{-1} \quad (5)$$

V_{rec} is the volume of the recombination region, while η_{ce} is a factor which accounts for a collisional enhancement of the $2s$ level population above the values predicted by pure recombination. Such an

enhancement can be determined from a comparison of the predicted two-photon spectrum with the observed UV continuum from HH objects. Dopita, Binette & Schwartz (1982) find values $2.8 \leq \eta_{ce} \leq 13.3$; interestingly, η_{ce} is found to be inversely proportional to the degree of excitation of the HH object as measured, e.g., from the $[\text{OIII}]5007\text{\AA}/[\text{OI}]6300\text{\AA}$ ratio. Eq. (5) makes the implicit assumption that the ionised clump is optically thin to the FUV radiation. It is easy to show that for typical dust grains of radius $0.1\mu\text{m}$ and density of 3 g cm^{-3} , the optical depth along the diameter of a spherical clump of radius r and particle density n can be written as:

$$\tau_\nu = 1.8 \cdot 10^{-8} Q_\nu n r d \quad (6)$$

where n is in cm^{-3} , r is in seconds of arc and the distance d is in parsecs. In the FUV range the absorption coefficient $Q_\nu \sim 1$ (Draine & Lee 1984), and for the typical parameters that we will derive (see Table 3) we obtain $\tau_{FUV} \sim 0.8$. We

emphasize that this number refers to the longest path across the clump, so only a small portion at the far side of the clump, with respect to any line of sight, will be only partially thick.

The FUV field emitted by the HH object is intercepted by the flow cavity walls, and a PDR is there formed. A fraction χ_c of the incident FUV field is predicted by PDR models (Tielens & Hollenbach 1985) to be reradiated via the [CII]158 μ m line; our observations allow us to determine (§ 3.3) values of χ_c in very good agreement with model predictions. Since we want to compare the predicted [CII]158 μ m line flux radiated by this PDR with our ISO-LWS observations, we are interested in the portion of the flow cavity which is encompassed by the instrument field of view. In other words, we need to estimate the fraction f_c of the L_{FUV} emitted by the HH object which is intercepted by the flow cavity in our LWS beam. The situation is sketched in Fig. 7, which serves as reference for the following discussion. R is the radius of the cavity, and R_b is the radius of the ISO-LWS beam. For simplicity, we will assume the HH object lying at the center of our coordinate system as pointlike with respect to R . The element solid angle at the cavity wall as seen from the origin is

$$d\Omega = \frac{R \, d\theta \, dz \, \cos \phi}{r^2} \quad (7)$$

where the $\cos \phi$ factor accounts for the projection, perpendicular to the line of sight from the origin, of the element area of the cavity wall. Expressing z and r as functions of R and ϕ , we obtain

$$d\Omega = \cos \phi \, d\phi \, d\theta \quad (8)$$

The total solid angle Ω_c under which the HH object sees the internal cavity walls (from $z=-R_b$ to $z=R_b$) is obtained by integrating Eq. (8) over 2π in $d\theta$, and from $-\arctan(R_b/R)$ to $\arctan(R_b/R)$ in $d\phi$. The FUV field is emitted isotropically, so that

$$f_c = \frac{\Omega_c}{4\pi} = \sin \left[\arctan \frac{R_b}{R} \right] \quad (9)$$

We can finally write the predicted flux of the [CII]158 μ m line from a system at the distance D as:

$$F_{CII} = \frac{10^{-7} \, L_{FUV} \, f_c \, \chi_c}{4\pi D^2} \, \text{Wcm}^{-2} \quad (10)$$

5. DISCUSSION

5.1. The Herbig-Haro Objects

To understand which are the critical parameters in our model, it is useful to show in Fig. 8 a diagnostic diagram that presents the relationship between our two observable quantities, F_{6cm} and F_{CII} , for various parameters sets. We will first consider the case of the HH objects, where Eq. (1) holds for the emitted radio continuum flux. For each grid in Fig. 8, the horizontal lines are sites of constant density (n in cm^{-3}) while the vertical lines indicates constant $\mathcal{R}=n/n_o$ compression ratio (density over pre-shock density). The full-line grid is computed for $v_s=100 \, \text{km s}^{-1}$, $\eta_{ce}=2$, $\chi_c=0.007$ and $r_{HH}=5''$. Decreasing the shock velocity to $70 \, \text{km s}^{-1}$ shifts the grid to lower radio fluxes (dashed), while a lower FUV \rightarrow CII, χ_c , conversion factor brings it down in [CII]158 μ m flux (dash-dotted, the opposite effect is obtained by raising the η_{ce} enhancement factor). Decreasing the radius of the HH object influences both quantities (dotted). We find no appreciable effect from the particular choice of the cavity radius R . It is reassuring that for reasonable choices of the model parameters we can reproduce the 6cm and [CII]158 μ m fluxes observed toward the HH objects. The number of free parameters in our model can be significantly decreased thanks to the available observational evidence. The value of χ_c for each object has been determined using our FIR continuum and [CII]158 μ m measurements (§ 3.3). The radius of the HH objects is taken from the radio maps of MRR93; the objects are clearly resolved, and the full size (after a tentative beam deconvolution) is $\sim 10''$. The value of η_{ce} is computed using its relationship (Dopita, Binette & Schwartz 1982) with the degree of excitation measured by the [OIII]5007Å/[OI]6300Å ratio; we use the [OIII]5007Å and [OI]6300Å line fluxes from HRR to derive values of 2 for the HH objects and 13 for the jet. We adopt shock velocities of $100 \, \text{km s}^{-1}$ for all HH objects from the measured [OIII]88.3 μ m/[NII]122 μ m ratio. Model results are weakly dependent on the cavity radius, for which we adopt a fiducial value of $R=10''$. We can then vary the plasma density and \mathcal{R} to fit the data, and the results are in Cols. 8-10 of Table 3.

For all HH objects we obtain densities which are below 10^4cm^{-3} , for which $2s \rightarrow 2p$ collisional population would depress the two-photon continuum due to Ly α decay. The presence of a transverse

TABLE 3

Model inputs and results for HH objects

Object	χ_c	r_{HH} ($''$)	R ($''$)	v_s (km s^{-1})	η_{ce}	FUV (G_0)	n (cm^{-3})	\mathcal{R}
HH 80	0.011	5	10	100	2	170	4200	13
HH 81	0.013	5	10	100	2	180	4500	10
HH 80N	0.007	5	10	100	2	670	8400	13

($\vec{B}_0 \perp \vec{v}_s$) magnetic field limits the compression ratio; we can write (Hollenbach & McKee 1979)

$$B_{0\perp} = 76.7 \left[\frac{v_s}{100 \text{ km s}^{-1}} \right] \sqrt{\frac{n}{\mathcal{R}^3}} \mu\text{G} \quad (11)$$

Using the parameters from Table 3 we see that $B_{0\perp}$ varies from 100 to 200 μG . We ran additional shock models using these large $B_{0\perp}$ values and found that the only way to reproduce the observed line ratios is to assume a pre-shock ionization fraction ≥ 0.5 . This is higher than the higher values (0.2-0.3) found toward several HH-jets by Bac-

ciotti & Eislöffel (1999); on the other hand the HH 80/81 flow is the most powerful in its class and may be peculiar in its ionization fraction as well.

5.2. The Jet

As far as the other positions along the jet are concerned, our model has less diagnostic power because of the high number of free parameters in the Reynolds (1986) model for radio emission from ionised jets.

Fig. 9 is the analogous for the jet of Fig. 8, where grids of models are plotted as a function

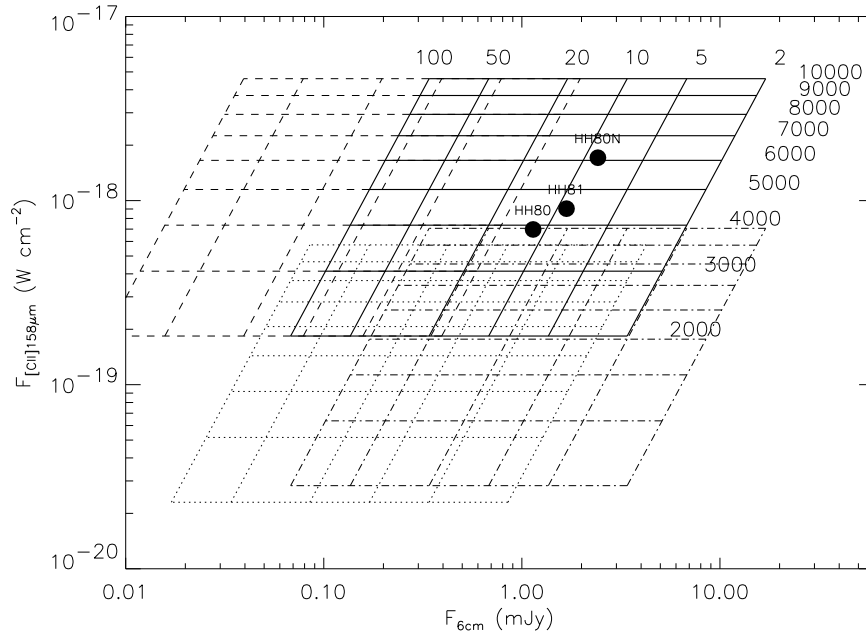


FIG. 8.— [CII]158 μm line flux as a function of 6 cm radio continuum flux (from Eq. 1) for different choices of HH model parameters. Each grid shows the locus of points of constant density n (horizontal lines) and constant $\mathcal{R}=n/n_0$ compression ratio. The full-line grid is computed for $v_s=100 \text{ km s}^{-1}$, $\eta_{ce}=2$, $\chi_c = 0.007$ and $r_{HH}=5''$. The other grids have $v_s=70 \text{ km s}^{-1}$ (dashed), $\chi_c = 0.002$ (dash-dotted) and $r_{HH}=2.5''$ (dotted). The full circles represent the observations.

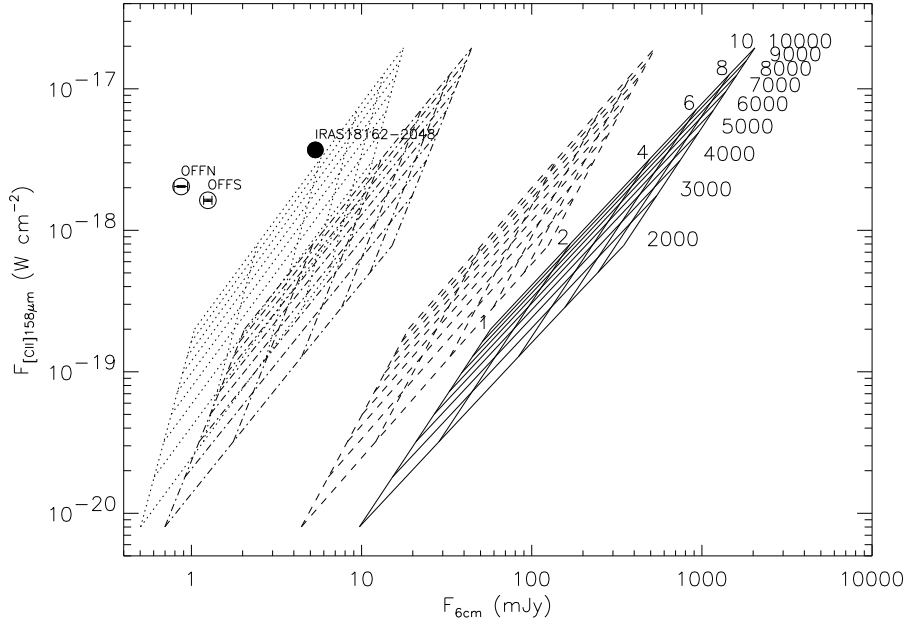


FIG. 9.— $[\text{CII}]158\mu\text{m}$ line flux as a function of 6 cm radio continuum flux (from Reynolds 1986) for different choices of jet model parameters. Each grid shows the locus of points of constant density n and jet's initial half-width in arcseconds. The full-line grid is computed for $[\epsilon, q_n, q_T, q_x] = [0.45, -0.9, -0.6, -0.5]$. The other grids have $q_T = -1$ (dashed), $\epsilon = 0.2$ (dash-dotted) and $q_n = -2$ (dotted). The circles represent the observations; the open symbols mean an uncertain assignment of the radio flux.

of density n in cm^{-3} and half-width w_0 , in arcseconds, of the jets at its base. While χ_c and η_{ce} are kept fixed to 0.002 (from our observations) and 13 (see above), the jet parameters are essentially free. The full-line grid represent the “pressure-confined” jet in Reynolds terminology, where the density, temperature and ionization radial gradients of the jet have values $[q_n, q_T, q_x] = [-0.9, -0.6, -0.5]$; in this particular jet the degree of collimation, expressed by a number ϵ which controls the jet's width as a function of radial distance ($w \propto r^\epsilon$), is $\epsilon = 0.45$. Another critical parameter, which we cannot independently fix, is the distance from the central source where the jet is injected; the full-line grid in Fig. 9 is obtained for $r_0 = 10 R_\odot$. This model predicts too much radio flux compared to the observations; other classes of standard models in Reynolds study are even less successful. Although of uncertain physical meaning, other combinations of the jet parameters can bring the predicted radio fluxes closer to the values observed along the HH 80/81 jet. Steepening the density gradient to $q_n = -2$ (dotted grid) will decrease the radio flux by more than an order of magnitude; a less pronounced effect

in the same direction is obtained by decreasing the temperature gradient to, e.g., $q_T = -1$ (dashed grid). Providing additional collimation by lowering ϵ down to, e.g., 0.2 (dashed-dotted grid), will also contribute to a better match between the model and the data. Finally, decreasing the jet-injection distance from the source, r_0 , will also work toward lowering the predicted radio flux. Although there is no single set of jet parameters that can fit the data, our model suggests steep density and/or temperature radial gradients along the jet, as well as a very high degree of collimation which is not ruled out by the observations (MRR93). Looking at the shape of the models grids in Fig. 9, it seems that a single jet model, i.e. a single model grid, cannot reproduce the $[F_{\text{CII}}, F_{6\text{cm}}]$ values of IRAS 18162-2048 and the two OFF positions. This is not due to the misalignment between the observed OFF positions and the jet axis. A better alignment would not have changed the radio flux (which we arbitrarily assigned based on the 6 cm map of MRR93); likewise, a half-LWS beam shift in the ISO observed positions would certainly not result in a one order of magnitude decrease of the $[\text{CII}]158\mu\text{m}$

line fluxes, as required to bring the OFF positions onto the model grid in Fig. 9. Rather, it is plausible that the central (brighter) portion of the jet considerably contributes to the FUV irradiation of the flow cavities at the two OFF positions. This would indeed correspond to increasing the assigned radio flux to the two OFF positions in Fig. 9.

5.3. The $F_{\text{CII}}-F_{6\text{cm}}$ relationship

Although it was one of the motivations to develop our model, one of the consequences of the model is that a $F_{\text{CII}}-F_{6\text{cm}}$ relationship is difficult to justify. The radio flux has a different origin in the HH objects and the jet, there is *a priori* no reason why IRAS 18162-2048 (where we model the radio flux as coming from a jet) should line up with the three HH objects (where we model the radio flux as coming from the post-shock region) in Fig. 6. The relative position of the HH objects themselves is also *a priori* depending on a high number of free parameters. Based on four points only, we must then conclude that the $F_{\text{CII}}-F_{6\text{cm}}$ relationship in Fig. 6 appears to be fortuitous. However, we will check for similar occurrences in other HH/jet systems where $[\text{CII}]158\mu\text{m}$ data are available and where the densities are low enough ($n \leq 10^4 \text{ cm}^{-3}$) that a shock/jet \leftrightarrow PDR connection can be expected.

6. CONCLUSIONS

We have performed a far-IR spectroscopic study of the HH 80/81 system. Line ratio analysis confirms for the first time the Herbig-Haro nature of the nebula HH 80N, which probably represents the head of the counterflow to HH 80 and 81. We reveal shock velocities of the order of 100 km

s^{-1} in correspondence with the HH objects, while lower excitation conditions appear to be present elsewhere along the radio jet. A comparison with proper motion velocities in excess of 600 km s^{-1} indicate that the shocks arise at the interface between two fast-moving flows.

Besides shock-excited emission, an important PDR contribution is present all along the bipolar flow, where densities below 10^4 cm^{-3} are also diagnosed. Using a simple model, we have provided quantitative arguments supporting the idea that the FUV field radiated by the ionised material of the recombination regions in the HH objects and of the jet emanating from IRAS 18162-2048, is able to induce the formation of a PDR in the immediately surrounding medium (i.e. the flow cavity walls). This would provide further evidence that the jet/HH own radiation field affects its surrounding medium in a measurable way. Attempts to model the chemistry of outflows should not ignore the influence of the radiation field of the shocks responsible for the acceleration of the outflow itself.

We thank Luis Felipe Rodríguez for kindly making available to us his 6 cm VLA map of the HH 80/81 region. We also thank the referee, Chris Davis, for his careful reading of the manuscript. The ISO Spectral Analysis Package (ISAP) is a joint development by the LWS and SWS Instrument Teams and Data Centers. Contributing institutes are Centre d'Etude Spatiale des Rayonnements (France), Institute d'Astrophysique Spatiale (France), Infrared Processing and Analysis Center (United States), Max-Planck-Institut für Extraterrestrische Physik (Germany), Rutherford Appleton Laboratories (United Kingdom) and the Space Research Organization, Netherlands.

REFERENCES

- Aspin, C., & Geballe, T.R. 1992, A&A, 266, 219
 Aspin, C., Puxley, P. J., Blanco, P. R., et al. 1994, A&A, 292, L9
 Bacciotti, F., & Eisloffel, J. 1999, A&A, 342, 717
 Beck-Winchatz, B., Böhm, K.H., & Noriega-Crespo, A. 1996, AJ, 111, 346
 Binette, L., Dopita, M.A., & Tuohy, I.R. 1985, ApJ, 297, 476
 Churchwell, E. 1998 in "The Origin of Stars and Planetary Systems", ed. C.J. Lada & N.D. Kylafis, p515
 Clegg, P.E., Ade, P.A.R., Armand, C., et al. 1996, A&A, 315, L38
 Curiel, S., Cantó, J., Rodríguez, L.F. 1987, Rev. Mexicana Astron. Af., 14, 595
 Davis, C.J., Dent, W.R.F., Burnell, S.J. 1990, MNRAS, 244, 173
 de Graauw, T., Haser, L.N., Beintema, D.A., et al. 1996, A&A, 315, L49
 Dopita, M.A., Binette, L., Schwartz, R.D. 1982, ApJ, 261, 183
 Draine, B.T. 1980, ApJ, 241, 1021
 Draine, B.T., Lee, H.M. 1984, ApJ, 285, 89
 Eisloffel, J., Mundt, R., & Böhm, K.H. 1994, AJ, 108, 1042
 Emerson, D. 1996, "Interpreting Astronomical Spectra", Wiley & Sons, Chichester, England
 Girart, J.M., Rodríguez, L.F., Anglada, G., et al. 1994, ApJ, 435, L145
 Girart, J.M., Estalella, R., Ho, P.T.P. 1998, ApJ, 495, 59
 Habing, H.J. 1968, Bull. Astr. Inst. Netherlands, 19, 421

- Hartmann, L. 1998 in “Accretion Processes in Star Formation”, Cambridge University Press, p.13
- Hartigan, P., Raymond, J., & Hartmann, L. 1987, *ApJ*, 316, 323 (HRH87)
- Heathcote, S., Reipurth, B., Raga, A. 1998, *AJ*, 116, 1940 (HRR)
- Herbig, G.H., & Jones, B.F. 1981, *AJ*, 86, 1232
- Hollenbach, D., McKee, C.F. 1979, *ApJS*, 41, 555
- Hollenbach, D., McKee, C.F. 1989, *ApJ*, 342, 306 (HM89)
- Hummer, D.G., Seaton, M.J. 1963, *MNRAS*, 125, 437
- Kaufman, M.J., Neufeld, D.A. 1996, *ApJ*, 456, 611
- Kessler, M.F., Steinz, J.A., Anderegg, M.E., et al. 1996, *A&A*, 315, L27
- ISO Handbook,
<http://www.iso.vilspa.esa.es/users/handbook/>
- Martí, J., Rodríguez, L.F., Reipurth, B. 1993, *ApJ*, 416, 208 (MRR93)
- Martí, J., Rodríguez, L.F., Reipurth, B. 1995, *ApJ*, 449, 184
- Martí, J., Rodríguez, L.F., Reipurth, B. 1998, *ApJ*, 502, 337
- Miller, G.E., Scalo, J.M. 1979, *ApJS*, 41, 513
- Molinari, S., Brand, J., Cesaroni, R., Palla, F. 2000, *A&A*, 355, 617
- Noriega-Crespo, A., Böhm, K.H., & Raga, A.C. 1989, *AJ*, 99, 1918
- Noriega-Crespo, A., Garnavich, P.M., Curiel, S., Raga, A.C., & Ayala, S. 1997, *ApJ*, 486, L55
- Nussbaumer, H., Schmutz, W. 1984, *A&A*, 138, 495
- Ogura, K. 1995, *ApJ*, 450, L230
- Pequignot, D. 1986 in “Workshop on Model Nebula”, Observatoire de Paris, D. Péquignot ed. p363
- Poetzel, R., Mundt, R., & Ray, T.P. 1989, *A&A*, 224, L13
- Pravdo, S.H., Rodríguez, L.F., Curiel, S., Cantó, J., Torrelles, J.M., Becker, R.H., Sellgren, K. 1985, *ApJ*, 293, L35
- Raga, A.C., & Böhm, K.H. 1986, *ApJ*, 308, 829
- Raga, A.C., Binette, L., Canto, J., & Calvet, N. 1990, *ApJ*, 364, 601
- Raga, A.C., Williams, D.A. 2000, *A&A*, 358, 701
- Reynolds, S.P. 1986, *ApJ*, 304, 713
- Reipurth, B., & Grahman, J.A. 1988, *A&A*, 202, 219
- Reipurth, B. & Heathcote, S. 1997 in “Herbig-Haro Flows and the Birth of Low Mass Stars”, ed. B. Reipurth & C. Bertout, p3
- Rodríguez, L.F., & Reipurth, B. 1989, *RevMexA&A*, 17, 59
- Rodríguez, L.F., Moran, J.M., Ho, P.T.P., & Gottlieb, E. W. 1980, *ApJ*, 235, 845
- Rodríguez, L.F., Curiel, S., Ho, T.P., Torrelles, J.M., & Cantó, J. 1990, *ApJ*, 352, 645
- Shepherd, D.S., Churchwell, E. 1996, *ApJ*, 472, 225
- Shull, J.M., McKee, C.F. 1979, *ApJ*, 227, 131
- Stone, J.M. & Norman, M.L. 1993, *ApJ*, 413, 210
- Tielens, A.G.G.M., Hollenbach, D. 1985, *ApJ*, 291, 722
- Torrelles, J.M., Rodríguez, L.F., Cantó, J., et al. 1992, *ApJ*, 396, L95
- Torrelles, J.M., Gómez, J.J., Ho, P.T.P., et al. 1993, *ApJ*, 417, 655
- Wolfire, M.G., Königl, A. 1993, *ApJ*, 415, 204
- Wolfire, M.G., Pound, M.W., Mundy, L., Lord, S.D. 2000, <http://wits.ipac.caltech.edu>